Published in final edited form as:
Astrophys J. 2018 February 20; 854(2): . doi:10.3847/1538-4357/aaa5a5.

Isotopic Dichotomy among Meteorites and Its Bearing on the Protoplanetary Disk

Edward R. D. Scott[1], **Alexander N. Krot**[1], and **Ian S. Sanders**[2]

[1] Hawai'i Institute of Geophysics and Planetology, University of Hawai'i, Honolulu, HI 96822, USA
[2] Department of Geology, Trinity College, Dublin 2, Ireland

Abstract

Whole rock $\Delta^{17}O$ and nucleosynthetic isotopic variations for chromium, titanium, nickel, and molybdenum in meteorites define two isotopically distinct populations: carbonaceous chondrites (CCs) and some achondrites, pallasites, and irons in one and all other chondrites and differentiated meteorites in the other. Since differentiated bodies accreted 1–3 Myr before the chondrites, the isotopic dichotomy cannot be attributed to temporal variations in the disk. Instead, the two populations were most likely separated in space, plausibly by proto-Jupiter. Formation of CCs outside Jupiter could account for their characteristic chemical and isotopic composition. The abundance of refractory inclusions in CCs can be explained if they were ejected by disk winds from near the Sun to the disk periphery where they spiraled inward due to gas drag. Once proto-Jupiter reached 10–20 $M_{\oplus}$, its external pressure bump could have prevented millimeter- and centimeter-sized particles from reaching the inner disk. This scenario would account for the enrichment in CCs of refractory inclusions, refractory elements, and water. Chondrules in CCs show wide ranges in $\Delta^{17}O$ as they formed in the presence of abundant ^{16}O-rich refractory grains and ^{16}O-poor ice particles. Chondrules in other chondrites (ordinary, E, R, and K groups) show relatively uniform, near-zero $\Delta^{17}O$ values as refractory inclusions and ice were much less abundant in the inner solar system. The two populations were plausibly mixed together by the Grand Tack when Jupiter and Saturn migrated inward emptying and then repopulating the asteroid belt with roughly equal masses of planetesimals from inside and outside Jupiter's orbit (S- and C-type asteroids).

comets: general

meteorites; meteors; meteoroids

minor planets, asteroids: general

planets

satellites: gaseous planets

protoplanetary disks

1. Introduction

Meteorites, excluding those from Mars and the Moon, are traditionally thought to be derived from planetesimals that formed in the main asteroid belt between the orbits of Mars and Jupiter, 2–4 au from the Sun (e.g., McSween & Huss 2010; Scott & Krot 2014; Johansen et al. 2015). However, two studies published in 2011 suggested that a major fraction of asteroids and meteorite parent bodies may not have formed in the asteroid belt.

First, Walsh et al. (2011), who were trying to explain the low masses of Mars and the asteroid belt, suggested in their so-called Grand Tack model that Jupiter formed at the snowline at 3.5 au and then migrated inward through the protoplanetary disk depopulating the asteroid belt. When Jupiter reached 1.5 au, Saturn, which migrated faster, caught Jupiter in a resonance and both planets reversed direction and migrated outward. This caused Jupiter to repopulate the asteroid belt with roughly equal masses of water-poor, S-type asteroids, which formed inside the snowline, and water-rich, C-type asteroids, which formed outside the snowline between the giant planets (Morbidelli et al. 2015).

The second hint that C-type asteroids might not be indigenous to the asteroid belt comes from variations of mass-independent isotopic compositions of meteorites for O, Cr, and Ti, which define two well-separated clusters. Carbonaceous chondrites and a few differentiated meteorites form one cluster and all other meteorites including ordinary and enstatite chondrites and lunar and Martian meteorites define the other (Warren 2011a, 2011b). Warren (2011a, 2011b) speculated that the two populations formed in the outer and inner solar system, respectively, noting that the Grand Tack model of Walsh et al. (2011) provides a possible mechanism for mixing the bodies that formed either side of Jupiter in the asteroid belt. However, Warren (2011a, 2011b) did not exclude the possibility that the isotopic dichotomy resulted from accretion of material to the disk after planetesimals had begun to form, rather than from radial variations in the disk. Note that even though the links between some meteorite and asteroid types are uncertain, carbonaceous chondrites probably come from C-type asteroids as the most abundant class among falls, CM2 chondrites (Krot et al. 2014), is closely linked spectrally to the dominant class of C-type asteroids, Cgh- and Ch-type (Burbine 2014). Ordinary chondrites are derived from some S-type asteroids (Nakamura et al. 2011). Enstatite chondrites are closely related to enstatite achondrites, which are probably derived from E-type asteroids that are especially abundant at the inner edge of the asteroid belt (Burbine 2014).

This study was triggered by the recent discovery that an unexpectedly large fraction of iron meteorites (5 of 14 groups plus ungrouped irons) are derived from the carbonaceous isotopic reservoir (Budde et al. 2016a; Kruijer et al. 2017). This increases the importance of understanding the isotopic dichotomy among meteorites and its implications for the origins of asteroids and meteorites.

We first review mass-independent isotopic data for meteorites, including data for newly discovered kinds of meteorites that have been published since Warren (2011a, 2011b) to establish better limits on the extent, and causes of the isotopic dichotomy (Section 2). In Section 3, we examine some properties of chondrules and refractory inclusions in chondrites

to see whether they support the existence of two isotopically distinct reservoirs. In Section 4, we discuss evidence that appears inconsistent with the derivation of meteorites and asteroids from separate inner and outer solar system populations. Finally, in Section 5, we discuss how and when the two isotopic populations were mixed together in the asteroid belt. Specifically, we address whether the isotopic dichotomy among meteorites supports the Grand Tack model.

2. Evidence for Two Isotopically Distinct Reservoirs in the Protoplanetary Disk from Mass-independent Isotopic Variations in Bulk Meteorites

Most mass-independent isotopic variations in meteorites that cannot be attributed to radioactive decay or spallation by cosmic rays reflect nucleosynthetic processes in dying stars, and a lack of homogenization of the grains that formed around such stars when they later converged to make the protosolar molecular cloud from which the meteorite parent bodies were assembled (Dauphas & Schauble 2016). (Oxygen isotopic variations are an important exception and are discussed below.) Mass-independent isotopic variations in presolar grains are typically very large, up to several orders of magnitude from solar system values (Zinner 2014). These grains, which are nanometers-to-micrometers in size, have been directly identified in the matrices of the most pristine chondrites at concentrations of up to ~100 ppm and are the ultimate source of mass-independent isotopic variations in objects like chondrules and refractory inclusions (Ca–Al-rich inclusions (CAIs), and amoeboid olivine aggregates (AOAs)), which formed in the solar system.

The largest nucleosynthetic isotopic variations in solar system objects are shown by CAIs, which formed at high temperatures (>1400 K) in a gas of solar composition. These inclusions, which are tens of micrometers to millimeters in size, are the oldest components in chondrites (Connelly et al. 2012). Typical CAIs, which are present at percent levels in carbonaceous chondrites, show isotopic variations that differ from terrestrial values by as much as a few permil (deviations in parts per thousand). Even larger isotopic anomalies are found in rare types of CAIs (called FUN—fractionation and unidentified nuclear effects—and UN), which probably formed before normal CAIs (Sahijpal & Goswami 1998; Kööp et al. 2016; Park et al. 2017). For Ca, Ti, Cr, Fe, and Ni, the isotopic anomalies in CAIs are found predominantly in neutron-rich isotopes (e.g., ^{48}Ca, ^{50}Ti, and ^{54}Cr). For heavier elements, the anomalies reflect variations in the relative amounts of *s*-, *r*-, and *p*-processes of nucleosynthesis (Dauphas & Schauble 2016).

Nucleosynthetic anomalies at levels of a few parts per 10^4 (ε units) were first found in bulk chondrites in the form of ^{50}Ti excesses (Niemeyer 1985, 1988). They have since been recognized for over 10 elements in all kinds of chondrites, with enstatite chondrites being the closest to the terrestrial composition and carbonaceous chondrites showing the largest anomalies (Burkhardt et al. 2011; Dauphas & Schauble 2016). Differentiated meteorites also show isotopic anomalies at the ε level, e.g., Ni, Mo, Pd, and W in iron meteorites (Dauphas et al. 2002; Burkhardt et al. 2011; Steele et al. 2011; Mayer et al. 2015; Budde et al. 2016a; Kruijer et al. 2017) and Cr and Ti in achondrites (Trinquier et al. 2007, 2009). Iron meteorites show notably diverse nucleosynthetic isotopic compositions ranging from those

in main group IAB irons, which have Earth-like Mo and Ru compositions, for example, to those in group IVB, which have large isotopic anomalies matching those in carbonaceous chondrites (Burkhardt et al. 2011; Steele et al. 2012; Fischer-Gödde et al. 2015; Worsham et al. 2017). In general, the isotopic variations in bulk meteorites are similar though smaller than those in CAIs and also taken to reflect variations in *s*-, *r*-, and *p*-products of nucleosynthesis. However, there are significant differences. For example, bulk isotopic compositions for Mo in most meteorites are depleted in *s*-process Mo relative to Earth, whereas most CAI patterns are enriched in *r*-process Mo (Burkhardt et al. 2011).

Detailed studies of CAIs show that their nucleosynthetic isotopic variations are due to processing of complex mixtures of nucleosynthetic products (e.g., Niederer & Papanastassiou 1984). For example, at least four distinct components are required to account for the nucleosynthetic isotopic variations of Ti in CAIs (Niemeyer & Lugmair 1984). Bulk carbonaceous chondrites appear to be a mixture of at least two Ti components: one in CAIs and a second in matrix and chondrules (Leya et al. 2009). For Cr, leaching experiments on whole chondrites suggest that there were three distinct carriers of Cr isotopic anomalies (Göpel et al. 2015). Zirconium nucleosynthetic anomalies in bulk chondrites also require several stellar sources (Akram et al. 2015).

Isotopic heterogeneity in solar system materials may result from heterogeneities in the molecular cloud core that collapsed to form the solar system (e.g., Dauphas et al. 2002). However, correlations in bulk chondrites between isotopic anomalies for nuclides that were generated by different processes suggest that the anomalies do not reflect the addition of material from a single stellar source such as a supernova. Instead the isotopic variability in meteorites was probably produced by mechanical or thermal processing of solids in the disk (Trinquier et al. 2009; Burkhardt et al. 2012; Burkhardt & Schönbachler 2015; Mayer et al. 2015). Isotopic anomalies in CAIs were originally attributed to reflect late injection of supernova ejecta into the cloud or the disk (e.g., McCulloch & Wasserburg 1978; Brennecka et al. 2013). However, thermal processing of presolar components may also explain the CAI anomalies (e.g., Trinquier et al. 2009; Akram et al. 2015; Peters et al. 2017). Thus, mass-independent isotopic effects in CAIs and bulk chondrites may have arisen when presolar grains or phases that inherited the isotopic signature of presolar grains were selectively evaporated and the vapor was partially lost.

Mass-independent oxygen isotopic variations among CAIs and chondrules (Figure 1) were once thought to be nucleosynthetic in origin (Clayton et al. 1973), but are now thought to reflect a chemical process in the molecular cloud and/or the disk. These processes include photochemical dissociation of CO (Clayton 2002; Yurimoto & Kuramoto 2004; Lyons & Young 2005), surface reactions on dust grains in the molecular cloud (Dominguez 2010), and lightning in the disk (Nuth et al. 2012). Enrichment of the heavier and rarer oxygen isotopes, ^{17}O and ^{18}O, is required to account for the very ^{16}O-depleted magnetite in so-called cosmic symplectite discovered in the ungrouped carbonaceous chondrite Acfer 094 (Sakamoto et al. 2007; Seto et al. 2008) as well as the evidence in many chondrites for asteroidal alteration by ^{16}O-poor aqueous fluids (Choi et al. 1998; Krot et al. 2015). The proximity of the CAI oxygen isotopic composition to that of the Sun on the three-isotope plot of $^{17}O/^{16}O$ versus $^{18}O/^{16}O$ (Figure 1) suggests that variations in the oxygen isotopic

compositions of chondrites and chondrules reflect the mixing of ^{16}O-rich refractory material, nebular dust with a composition near the terrestrial fractionation line, and ^{17}O- and ^{18}O-enriched water ice (Krot et al. 2010; Tenner et al. 2015). The composition of the nebular dust might have been inherited from the molecular cloud (Krot et al. 2010) or it may have been acquired during thermal processing in the protoplanetary disk (Lugaro et al. 2012; Alexander et al. 2016). Bulk oxygen isotopic variations of meteorites have long been used to investigate their genetic relationships (Clayton 2004; Greenwood et al. 2017). Combining oxygen isotopic data with nucleosynthetic isotopic data for Cr, Ti, and Ni has provided even deeper insights into genetic relations among meteorites (Warren 2011a, 2011b).

The isotopic dichotomy among meteorites is best illustrated on a plot of Δ^{17}O versus ε^{54}Cr. (Δ^{17}O is the vertical displacement from the terrestrial mass fractionation line on the three-isotope plot (Figure 1) and is a useful measure of the mass-independent oxygen isotopic variation.) Figure 2 shows an updated version of this plot with data for 39 types of meteorite and Mars, the Moon and Earth. These probably come from 41 distinct bodies. (Acapulcoites and lodranites probably come from the same body; Krot et al. 2014.) The names of the meteorite groups and of ungrouped meteorites and the sources of the data are given in the Appendix. What is impressive is that the extent of the gap between the two clusters of data has scarcely diminished since Warren (2011a, 2011b) even though the number of bodies represented has increased from 27 to 41. In addition, the dichotomy defined by the chondrites is clearly visible among a wide variety of types of differentiated meteorites, including achondrites, pallasites, and iron meteorites.

Figure 3 shows a ε^{54}Cr versus ε^{50}Ti plot. Although the number of data points has increased only marginally since Warren (2011a, 2011b), the extent of the isotopic dichotomy between “carbonaceous” and “non-carbonaceous” isotopic reservoirs on this plot is impressive. The variations in the ε^{50}Ti values for carbonaceous chondrites plausibly reflect the addition of small amounts of CAIs as CAIs are enriched 20-fold in Ti and typically have ε^{50}Ti values of ~5–12 (Trinquier et al. 2009; Davis et al. 2016). The ε^{54}Cr enrichments in carbonaceous chondrites are not due to CAIs, which lack chromium, but appear to be due to nano-spinels of supernova origin (Dauphas et al. 2010; Qin et al. 2010), and correlate with the depletion of moderately volatile elements (Trinquier et al. 2009). They also correlate with mass-dependent variations in δ^{66}Zn, possibly due to loss of sulfides in the disk (Pringle et al. 2017). Trends for non-carbonaceous meteorites in Figures 2 and 3 are unlike those in carbonaceous chondrites and clearly reflect processing of different components. Thus, the three variables plotted in Figures 2 and 3 were controlled by different processes suggesting that the isotopic dichotomy reflects important differences in the formation history of the two populations.

Few iron meteorites have been analyzed for Cr, Ti, and O isotopes, but their Mo isotopic compositions confirm that they fall into two populations, which are linked to the carbonaceous and non-carbonaceous chondrites. On a plot ε^{95}Mo versus ε^{94}Mo, most iron meteorite groups, including IAB, IIAB, IIIAB, and IVA, plot on a line with the non-carbonaceous chondrites due to variable deficits in *s*-process Mo relative to the terrestrial composition (Budde et al. 2016a). However, five small groups—IIC, IID, IIF, IIIF, and IVB —and a number of ungrouped irons plot on a subparallel line defined by the bulk Mo

isotopic compositions of the carbonaceous chondrites (Budde et al. 2016a; Kruijer et al. 2017; Poole et al. 2017; Worsham et al. 2017). The offset of the second line reflects an excess of *r*-process Mo, and the spread along this line is also due to a deficit of *s*-process Mo. Thus, a significant fraction of iron meteorites was derived from the carbonaceous chondrite reservoir.

Given the wide variety of meteorite types that exhibit isotopic dichotomy (Figure 2), and the links between major asteroid types and meteorite types noted above, it seems unlikely that the isotopic dichotomy is an artifact due to poor sampling of the asteroid belt. Temporal or spatial variations in the disk are probably responsible (Warren 2011a, 2011b; Sugiura & Fujiya 2014). Alexander (2017) argued that continued accretion to the disk caused temporal variations as the carbonaceous chondrites, which show large isotopic anomalies, formed later than other solar system samples. However, the parent bodies of the carbonaceous chondrites started to accrete around 2.5 Myr after the formation of typical CAIs (Doyle et al. 2015; Krot & Nagashima 2017), yet the isotopic dichotomy already existed ~0.5–1 Myr after CAI formation when the parent bodies of the iron meteorites accreted (Kleine & Wadhwa 2017; Kruijer et al. 2017). Thus, the isotopic dichotomy is most plausibly attributed to the accretion of meteorite parent bodies in two very distinct locations in the disk.

To summarize, nucleosynthetic isotopic variations are endemic in bulk meteorites and are probably relicts caused by thermal processing in the disk of presolar grains and carriers of their isotopic signatures. Carbonaceous chondrites, which also acquired nucleosynthetic signatures from CAIs, are isotopically distinct from all other chondrites including ordinary and enstatite chondrites. Differentiated meteorites can also be divided into two populations that are related to carbonaceous and non-carbonaceous chondrites. They include achondrites, pallasites, and irons, and appear to have inherited their nucleosynthetic signatures from precursor chondritic materials that melted so they are not represented among actual chondritic meteorites today. Given the extent of the isotopic dichotomy (Figures 2 and 3), the wide range of chondritic and differentiated meteorites that show the dichotomy, and their extended accretion period, it seems clear that the isotopic dichotomy reflects spatial variations in the disk that existed soon after planetesimals began to accrete and that the two populations were isolated for several megayears. A plausible reason for the isolation of the two populations is that they were separated by a large protoplanet. Although protoplanets may have formed in the asteroid belt (O'Brien et al. 2007), it seems unlikely that a single protoplanet could have created such impressive isotopic bimodality in the asteroid belt. Formation of the two populations on either side of Jupiter seems much more likely. In the next section, we look at the components in chondrites to see whether formation and accretion of chondrites on either side of Jupiter can help explain some of their diverse properties.

3. Isotopically Distinct Reservoirs: Evidence from Chondritic Components

3.1. Refractory Inclusions

Refractory inclusions (CAIs and AOAs) are thought to have formed very early close to the Sun where they were exposed to high temperatures and irradiation by solar energetic particles (McKeegan et al. 2000; Scott & Krot 2014). The general similarities in the

chemical and isotopic compositions of refractory inclusions from different chondrite groups and the large difference in isotopic compositions between refractory inclusions and chondrules (e.g., Figure 1), suggest that refractory inclusions in *different* chondrites formed under similar conditions and were transported outward to the different disk regions where chondrules, chondrites, and comets formed (e.g., Lin et al. 2006; Krot et al. 2009; Brownlee et al. 2012). Here we address two questions. Why are refractory inclusions much more abundant in carbonaceous chondrites than in enstatite and ordinary chondrites (Scott & Krot 2014) even though carbonaceous chondrites clearly accreted farther from the Sun (Rubin 2011)? How did refractory inclusions survive in the disk for 3 Myr so that they could accrete with late-forming chondrules?

Various hypotheses have been proposed to answer these questions. Some authors have argued that refractory inclusions and chondrules were both radially transported above the disk from near the Sun via X-winds (Shu et al. 1996) or disk winds (Salmeron & Ireland 2012; Van Kooten et al. 2016), contrary to chemical and isotopic evidence that they formed under very different conditions (e.g., Figure 1). In addition, the Al–Mg radiometric ages of chondrules appear to be 2–3.5 Myr younger than those of CAIs, assuming that ^{26}Al, which has a half-life of 0.7 Myr, was uniformly distributed in the disk after a brief epoch of CAI formation (Ushikubo et al. 2012; Nagashima et al. 2018). (Some Pb–Pb ages of chondrules are as old as those of CAIs, but most chondrules have Pb–Pb ages that are 1–3 Myr younger than CAIs; Nagashima et al. 2018.) Liffman et al. (2016) have proposed that CAIs were transported outward by centrifugal ejection from the gas accreted to the protosun. Other models invoke turbulence caused by the magnetorotational instability to transport refractory inclusions and angular momentum outward at the disk midplane (Cuzzi et al. 2003; Ciesla 2007, 2010). However, the main agent for transferring angular momentum in the disk is now thought to be disk winds rather than turbulent viscosity (e.g., Morbidelli & Raymond 2016). If carbonaceous chondrites were the first to form, their high abundance of refractory inclusions could simply be attributed to aerodynamic redistribution of chondritic components in the disk (Jacquet et al. 2012; Jacquet 2014). However, ^{26}Al–^{26}Mg radiometric ages of chondrules in chondrites (Kita & Ushikubo 2012; Nagashima et al. 2018) and thermal modeling of parent asteroids (Sugiura & Fujiya 2014) suggest that ordinary chondrites formed before carbonaceous chondrites.

The most plausible explanation for the higher abundance of refractory inclusions farther from the Sun is that they were transported from their formation region by disk winds (Figure 4). Observations using the Atacama Large Millimeter/submillimeter Array (ALMA) show that disk wind velocities may exceed 5 km s^{-1} near the inner edge of the disk and might have ejected refractory inclusions (Bjerkeli et al. 2016). The wide opening angle of outflows in some disks (Ruiz-Rodriguez et al. 2017) could have ensured that some ejected solids were deposited in the outer, flared regions of the solar disk. Like Gerber et al. (2017), who also favor formation of carbonaceous chondrites outside Jupiter, we infer that refractory inclusions were deposited in the outermost parts of the disk and prevented from spiraling into the inner solar system by Jupiter.

Although there is no consensus about Jupiter's formation, it is plausible that the growth of Jupiter's core to ~10–20 $M_{\oplus}$ took only a few 10^5 years when it would have started to accrete

gas, creating a local minimum in the gas pressure (Lissauer et al. 2009; Helled et al. 2013; Lambrechts et al. 2014). Solid particles in the disk would have spiraled inward under gas drag as the gas orbited at sub-Keplerian velocity. However, in the annulus outside Jupiter's orbit, where the pressure gradient was reversed, the gas would have rotated at super-Keplerian velocity, causing solid particles to migrate outward (Weidenschilling 1977). Refractory inclusions are plausibly most abundant in CV and CO carbonaceous chondrites because their planetesimals accreted just outside the orbit of proto-Jupiter near a pressure bump. The same process may have prevented ice particles from drifting inward beyond proto-Jupiter and would have helped to keep the inner solar system relatively dry (Morbidelli et al. 2016). Since the carbonaceous chondrites continued to accrete until >3 Myr after CAI formation (Kita & Ushikubo 2012; Doyle et al. 2015; Nagashima et al. 2018), their parent bodies could not have been scattered into the asteroid belt before that time. This is consistent with models for Jupiter's formation in which the gaseous envelope accreted slowly over several megayears until its mass exceeded that of the core and gas accreted rapidly (Helled et al. 2013).

Carbonaceous chondrites differ from other chondrites as they have higher concentrations of refractory elements like Ca, Al, and Ti (e.g., Krot et al. 2014). The correlation between CAI abundance in carbonaceous chondrite groups and Ca abundance normalized to Mg to allow for diverse volatile contents (Figure 5) probably reflects the addition of CAIs (Hezel et al. 2008; Rubin 2011). Ebel et al. (2016) have questioned this conclusion as CO chondrites scatter off the trend. Nevertheless, it seems plausible that the concentration of CAIs in the giant planet region by disk winds and proto-Jupiter can account for their diverse ε^{50}Ti excesses (Figure 3) as well as their abundances of CAIs and refractory elements (Figure 5). Ordinary and enstatite chondrites have the lowest abundances of refractory elements as well as very low abundances of CAIs. Rumuruti-type chondrites have slightly higher refractory and CAI abundances (Bischoff et al. 2011).

3.2. Chondrules

If carbonaceous and non-carbonaceous chondrites formed on opposite sides of Jupiter, as inferred above, we might expect to see some differences in the isotopic compositions of their chondrules. Given the large number of chondrules that have been analyzed for oxygen isotopes in the least metamorphosed and altered chondrites in various groups, we focus first on oxygen data. Figure 6 shows data for chondrules in CR chondrites (Tenner et al. 2015) and two ungrouped carbonaceous chondrites, Acfer 094 (Ushikubo et al. 2012) and Yamato (Y) 82094, which are related to CO chondrites (Tenner et al. 2017). Chondrules in CV chondrites (Hertwig et al. 2016) and CM chondrites (Chaumard et al. 2016, 2017) show similar trends and are not plotted here. Although some chondrules contain relict silicates, which did not crystallize from the host chondrule melt and have very different isotopic compositions, olivine and pyroxene grains in individual chondrules in carbonaceous chondrites typically have indistinguishable isotopic compositions within analytical uncertainties (e.g., Hertwig et al. 2016). Ion probe analyses of olivines and pyroxenes are therefore good proxies for the bulk chondrule compositions. Figure 6 shows that chondrules in carbonaceous chondrites plot along the slope 1 reference line called PCM (primitive chondrule mineral; Ushikubo et al. 2012). In each chondrite, the chondrules show a large

spread of $\Delta^{17}O$ values, typically from −6‰ to −1‰ (except CH and CB) although each is isotopically homogeneous. Most of the spread in $\Delta^{17}O$ values has been attributed to the addition of ^{16}O-poor water vapor to the gas and contamination of chondrule melts with ^{16}O-rich olivines from AOAs (Tenner et al. 2017).

Oxygen isotopic data for chondrules in three non-carbonaceous chondrites are shown in Figure 6: LL ordinary chondrites (Kita et al. 2010), EH and EL3 chondrites (Weisberg et al. 2011), and the Kakangari meteorite, which is classified as a K3 chondrite (Nagashima et al. 2015). (We classify the K chondrite grouplet as non-carbonaceous based on low refractory abundances (sub CI; Krot et al. 2014), isotopic analyses of Kakangari for titanium by Niemeyer 1985, oxygen by Weisberg et al. 1996, calcium by Prombo & Lugmair 1987 and the $\Delta^{17}O$ versus $\varepsilon^{50}Ti$ and $\varepsilon^{48}Ca$ versus $\varepsilon^{50}Ti$ plots of meteorite data by Dauphas & Schauble 2016.) Chondrules in unequilibrated H and R chondrites are almost identical in oxygen isotopic composition to those in the LL chondrites (Kita et al. 2008, 2013, 2015). Figure 6 shows that chondrules in the non-carbonaceous chondrites plot on or near the terrestrial fractionation line and the extent of mass fractionation parallel to the line is much larger than in carbonaceous chondrites. This difference between the oxygen isotopic compositions of chondrules in carbonaceous and non-carbonaceous chondrites is entirely consistent with the formation of these two kinds of chondrite, and their chondrules, either side of Jupiter. Carbonaceous chondrites show a significant spread in $\Delta^{17}O$ values due to the ubiquity in the outer solar system of ^{16}O-rich grains from refractory inclusions, which seem to be deficient in the inner solar system, and to ^{16}O-poor water ice, which appears to be abundant in the outer solar system (Krot et al. 2015).

The oxygen isotopic compositions of chondrules in carbonaceous and non-carbonaceous chondrites show very little overlap (Figure 6). There is some overlap in the composition of chondrules in ordinary chondrites and CR (Renazzo-type) carbonaceous chondrites, for example, but the ^{16}O-poor chondrules in CR chondrites typically have higher FeO contents. Among non-carbonaceous chondrites, there is little overlap in composition between chondrules in ordinary, enstatite, and K chondrites, suggesting that they formed in separate locations.

Oxygen isotopic compositions of chondrules are consistent with the observation that chondrules from different chondrite groups have petrologic properties including size, texture, and chemical compositions, suggesting that there were many distinct populations of chondrules in different parts of the disk (Jones 2012). However, Olsen et al. (2016) found appreciable variations in the $\mu^{54}Cr$ isotopic variations (deviations from the terrestrial value in parts per million) among chondrules in CV (Vigarano-type) carbonaceous chondrites and inferred that they had formed throughout the inner and outer solar system and had been transported large distances to the region where CV chondrites accreted. Gerber et al. (2017), who studied the Ti isotopic compositions of chondrules in various chondrite groups, argued against this interpretation and attributed the large range of $\varepsilon^{50}Ti$ values in chondrules in CV and CR chondrites and the relative homogeneity of chondrules in ordinary and enstatite chondrites to an admixture of CAI-like material to enstatite and ordinary chondrite-like chondrule precursors. Thus, both isotopic and petrologic data can be interpreted in terms of chondrule formation at various radial distances from the Sun in regions that were isolated

from each other. This is consistent with the view that chondrules formed in distinct nebular regions with high dust-gas ratios with very little mixing between regions (Jones 2012). This dust accreted with chondrules to form the chondrite matrix material. Nucleosynthetic anomalies for Mo and W show a complementary relationship between chondrules and matrix in the Allende CV chondrite (Budde et al. 2016a, 2016b). This probably resulted from the transfer of metal grains enriched in s-process Mo and W from chondrules to matrix, or metal grains depleted in s-process Mo and W from matrix to chondrules during chondrule formation. Thus, dust that was present when chondrules formed accreted with chondrules to form chondrites. Each chondrite group contains components that, except for the refractory inclusions, were locally produced in the disk. Early formation of protoplanets minimized mixing between chondrite types.

4. Possible Counter Arguments

In Section 3, we argued that early formation of proto-Jupiter was probably responsible for the dichotomy in the distribution of mass-independent isotopic variations in meteorites and the abundance of CAIs and water in carbonaceous chondrites. The homogeneity of oxygen and titanium isotopes in chondrules in non-carbonaceous chondrites and the heterogeneity of these isotopes in carbonaceous chondrite chondrules are probably due to the higher abundance of refractory material (and ^{17,18}O-rich water) outside of Jupiter's orbit. In Section 4.1, we discuss evidence that appears inconsistent with these conclusions.

4.1. Stratified Structure of the Asteroid Belt

The classical plot of asteroid type versus semimajor axis shows a highly stratified asteroid belt with an orderly compositional gradient, suggesting that each type formed at a specific location (Gradie & Tedesco 1982; Burbine 2014). E-type asteroids appear to dominate at <2 au, S-types at ~2.1–2.3 au, C-types at 2.5–3.5 au, and D-types at 4–5 au. This concept of a highly stratified belt is not supported by recent data for smaller asteroids 5–100 km in size, indicating that all asteroid types exist in every region of the main belt (De Meo & Carry 2014). This distribution cannot be simply attributed to the Yarkovsky effect, as the drift rate is too slow: only ~0.03 au in 4.5 Gyr for 20 km wide bodies and ~0.1 au for 5 km bodies (Bottke et al. 2002). The ranges of orbital parameters among asteroid families are truncated by strong resonances, suggesting that the combined effects of impacts and Yarkovsky effect are not sufficient to spread bodies of this size across the whole asteroid belt. The trend of increasing C-type/S-type ratios with increasing distance from the Sun appears to be compatible with the Grand Tack model (Walsh et al. 2011, 2012) and does not require that C-type asteroids formed in the belt. The predominance of large P- and D-type asteroids between 3.6 and 5.4 au and small Ps and Ds throughout the asteroid belt probably results from the giant planet instability, which scattered cometary bodies across the belt after the gas in the disk had disappeared (Vokrouhlickyí et al. 2016).

The concept of a spectrally stratified asteroid belt and consideration of the thermal effects of ^{26}Al also led to the idea that the asteroid belt was also "thermally stratified" with the outer belt containing the least metamorphosed asteroids, which accreted late and the inner belt consisting of strongly heated asteroids, which accreted early (Bell et al. 1989; Grimm &

McSween 1993; Ghosh et al. 2006). When S-type asteroids were recognized as metamorphosed, unmelted asteroids, Bottke et al. (2006) suggested that iron meteorites were derived from bodies that formed in the terrestrial planet region. Higher impact rates inside 2 au offered one explanation for the early destruction of the parent bodies of iron meteorites (Scott et al. 2015). However, the nucleosynthetic isotopic variations among iron meteorites suggest that the concept of a single “accretion wave” that swept across the belt (Grimm & McSween 1993) is incorrect. Planetesimals that formed early and melted appear to have accreted in the inner and outer regions of the solar system, where chondrites also formed.

4.2. CAIs in CI Chondrites and Comet 81P/Wild 2

Since CI (Ivuna type) chondrites are thought to have formed outside the CV and CM (Mighei type) chondrite-forming region (Rubin 2011) and possibly close to the comet-forming region (Gounelle et al. 2008), their low concentration of CAIs, <0.05 vol.% (Figure 5), is puzzling. If CAIs were ejected from close to the protosun to the outermost parts of the protosolar disk (Figure 4), we should expect that the CAI abundance in CI chondrites would be comparable to that in comets, which probably formed beyond the giant planets (Brasser & Morbidelli 2013). Returned samples of comet 81P/Wild 2 and chondritic porous interplanetary particles, which are probably derived from comets, contain ~0.5–1 vol.% CAIs (Joswiak et al. 2017), consistent with external transport of CAIs to the outermost regions of the disk.

Evidence that CI chondrites once contained a higher volume of CAIs has been discovered from the distribution of thulium (Tm) and other rare-Earth elements (REEs) in meteorites and planets (Barrat et al. 2016). Because REEs have very similar geochemical behavior, their abundances in rocks when plotted in order of increasing atomic number are smooth functions of atomic number, after normalization to the REE concentrations in CI chondrites, which provide our best estimate for the composition of the nonicy solids in the disk (Palme et al. 2014). High-precision analyses of solar system materials for REEs that are normalized to CI chondrite abundances show a small excess or depletion of Tm relative to neighboring REE in the periodic table. Thulium exhibits a 1%–10% excess in carbonaceous chondrites but a deficiency of ~2% in non-carbonaceous chondrites, differentiated meteorites, and rocks from Earth and Mars (Dauphas & Pourmand 2015; Barrat et al. 2016).

Thulium excesses in carbonaceous chondrites are largest in the CV group and clearly result from the presence of a few percent of CAIs with so-called group II REE patterns (MacPherson 2014). Unlike other CAIs, which have flat REE patterns, group II CAIs, which comprise about half of all CAIs, are strongly depleted by factors of 3–10 in heavy REEs—except for Tm, which is undepleted—as they lack the so-called ultra-refractory CAI component. Thus, Tm bulk analyses are very sensitive to the presence of CAIs. Bulk REE patterns for CV chondrites mimic those of group II CAIs and the magnitude of their Tm excess is consistent with the presence of a few percent of group II CAIs (Stracke et al. 2012; Barrat et al. 2016). To account for the Tm deficiencies of ~2% in the normalized compositions of inner solar system materials, Barrat et al. (2016) argued that CI chondrites, the standard used for normalization, contain a corresponding Tm excess, which would require ≈1% CAIs in CI chondrites. We infer that the CAIs in CI chondrites were almost

entirely obliterated by extensive alteration and impact fragmentation in CI chondrites (Morlok et al. 2006). This is consistent with the study of the only known CAI in CI chondrites, which was partly altered (Frank et al. 2017), the micrometer-sized corundum and hibonite grains with CAI-like oxygen isotopic compositions in CI acid residues (Makide et al. 2011), and the olivine and pyroxene grains in CI chondrites, which have oxygen isotopic compositions indicating that they are derived from fragmented and altered chondrules like those in other carbonaceous chondrites (Leshin et al. 1997 Figure 6). Thus, we infer that all the bodies that formed outside Jupiter's orbit accreted a few percent of refractory inclusions and larger amounts of chondrules

4.3. Evidence for Mixing from Stardust Comet Samples

Studies of the returned 2–50 μm-sized cometary dust particles by the Stardust mission to comet 81P/Wild 2 revealed a large fraction of chondrule fragments and crystalline mineral grains resembling those in chondrites (e.g., Westphal et al. 2009; Brownlee et al. 2012). Olivine compositions and oxygen isotopic analyses suggest that this material was derived not from a single chondrite source but from various carbonaceous and ordinary chondrite-forming regions (Brownlee et al. 2012; Frank et al. 2014). This has been interpreted as "strong evidence of large-scale transport of solids across the full dimension of the protosolar nebula" (Brownlee 2014). Assuming that chondrules and chondrule fragments in Wild 2 originated in the inner solar system and that ^{26}Al was initially uniformly distributed in the protoplanetary disk at the canonical level ($^{26}Al/^{27}Al \sim 5 \times 10^{-5}$), and the fact that the only chondrule measured for Al–Mg systematics showed no evidence for radiogenic ^{26}Mg excess, Ogliore et al. (2012) inferred that Jupiter formed ≥3 Myr after CAIs.

These arguments assume the traditional view that chondrules and chondrites formed in the asteroid belt. However, if chondrules and chondrites also formed in the giant planet region, as suggested by the isotopic dichotomy, there is no need to invoke large-scale transport of thermally processed solids and late formation of Jupiter. Oxygen isotopic compositions of silicate fragments in Wild 2 are most similar to those of chondrules in CR chondrites (Nakashima et al. 2012), although they are deficient in type I chondrule fragments (Frank et al. 2014). We suggest that either these chondrules formed outside the giant planets or else comets contain predominantly CR chondrule fragments from just inside the comet-forming region.

4.4. D/H Ratios of Comets and Chondrites

Alexander et al. (2012) observe that the estimated deuterium/hydrogen (D/H) ratios of water in carbonaceous chondrites are much lower than those in Oort cloud comets and infer that carbonaceous chondrites could not be derived from the giant planet region, as the Grand Tack model requires. However, Oort cloud comets are probably derived from the trans-Neptunian region, like Kuiper Belt comets (Brasser & Morbidelli 2013). Alexander (2017) infers from the D/H ratios of Titan and Enceladus that carbonaceous chondrites formed inside 3–7 au. However, Morbidelli et al. (2015) note that there are problems inferring the radial variation of D/H in the disk from atmospheres of planetary satellites as circumplanetary disks evolve separately from the protosolar disk. In addition, D/H ratios can readily be modified by non-nebular processes. For example, the D/H ratio of Rumuruti type

and ordinary chondrites is higher than that in comets, which Alexander et al. (2012) attribute to iron oxidation in their parent bodies.

4.5. Water in Chondrites

If carbonaceous and non-carbonaceous chondrites formed on opposite sides of the snowline, where Jupiter formed, why do some carbonaceous chondrites have relatively low water and carbon contents like those in some non-carbonaceous chondrites? CM, CI, and CR chondrites have the highest contents of water and carbon among chondrites, but CO and CV have lower amounts that are comparable to those in some of the least metamorphosed ordinary chondrites (Krot et al. 2014). Krot et al. (2015) infer that CI, CM, and CR chondrites were altered under water/rock mass ratios of up to 0.6, whereas CV and CO chondrites were altered at lower water/rock ratios of 0.1–0.2.

We do not know the answer to this issue but note that water contents of carbonaceous chondrites are related to matrix contents and that the coarse-grained matrix material likely contained more water than the fine-grained matrix rims. Thus, the low water content of CO and CV chondrites may reflect their low content of coarse-grained matrix material relative to CI, CM, and CR chondrites (Scott & Krot 2014). We also note that comets can contain more rock than ice (Brownlee 2014; Davidsson et al. 2016), much less ice than the predicted theoretical water-rock ratio beyond the snowline of 1.2 (Krot et al. 2014; Palme et al. 2014).

5. How and When Were the Two Isotopic Populations Mixed Together in the Asteroid Belt?

The isotopic dichotomy in the solar system lasted until at least 3–4Myr after CAI formation, the likely accretion time of CR chondrites, which are the least metamorphosed and altered chondrites and have the highest concentration of presolar grains (Zhao et al. 2013; Budde et al. 2017; Krot & Nagashima 2017). The two isotopic populations were then intermixed, most likely by the migration of the giant planets before the gas had dissipated in the disk. In the Grand Tack model, once Jupiter and Saturn reached masses of ~50 $M_{\oplus}$, they migrated inward across the asteroid belt so that it was first emptied and then repopulated with S-type asteroids, which formed in the belt, and C-types, which formed outside Jupiter (Walsh et al. 2011). Alternatively, planetesimals from the giant planet region may have been scattered into the asteroid belt as a natural side-effect of the growth of giant planets (Kretke et al. 2017; Raymond & Izidoro 2017). Raymond & Izidoro (2017) show that scattering during the rapid growth of the gaseous envelopes of giant planets would have scattered nearby planetesimals in all directions and may have delivered water to the growing Earth. However, the Grand-Tack model has the advantage that it creates a strongly mass-depleted belt with roughly equal masses of S- and C-types, which both have excited orbits. Scattering by the giant planets without the Grand Tack does not explain the low mass of the asteroid belt, the roughly equal masses of S- and C-type asteroids, and the similar degree of excitation of C- and S-type orbits.

Chondrules and metal grains in CB metal-rich carbonaceous chondrites differ from those in other chondrites mineralogically, chemically, and isotopically, and they probably formed

from a gas-melt plume produced by a highly energetic collision 4.8 ± 0.3 Myr after CAIs (Krot et al. 2009; Bollard et al. 2015). Johnson et al. (2016) argue that the impact velocity necessary to partially vaporize the metallic core of a differentiated asteroid (Oulton et al. 2016), 18 ± 5 km s^{-1}, was the result of a spike in impact velocities lasting ~0.5 Myr, which was triggered by a Grand-Tack-like migration of Jupiter and Saturn across the asteroid belt. The presence of ordinary chondrite clasts within the CB chondrites, Bencubbin and Weatherford (Weisberg et al. 1990; Prinz et al. 1993), shows that ordinary chondrite fragments were mixed into the impact plume, like CAIs. (Bencubbin and Weatherford are not fragmental breccias that acquired clasts in a regolith long after they formed.) This strongly supports formation of the CB chondrites when the giant planets amalgamated the carbonaceous and non-carbonaceous populations in the asteroid belt.

Another unique type of impact occurred 4–6Myr after CAIs when the parent body of the ureilites, which was ≥ 125 km in radius, was catastrophically disrupted and broken into meter-sized fragments that cooled from 1100 °C to below 800 °C in days to months (Goodrich et al. 2004; Bischoff et al. 2014; Goodrich et al. 2015). In a conventional event, the short interval between breakup and reaccretion of impact debris and the likelihood that the debris cloud would be dusty and opaque suggest that hot fragments would not cool significantly before they reaccreted (e.g., Haack et al. 1996). However, if nebular gas had been present when the ureilite parent body was disrupted, the gas would damp debris orbits, aid accretion via pebble accretion, and allow for longer accretion times and greater heat loss from hot fragments. Reaccretion during or after a spike in impact velocities in the asteroid belt would also help explain the extraordinary variety and abundance of clasts in the Almahata Sitta ureilite breccia, including ordinary, enstatite, Rumuruti, and carbonaceous chondrite clasts (Herrin et al. 2010; Horstmann & Bischoff 2014; Goodrich et al. 2015; Fioretti et al. 2017). However, the presence of clasts with a range of Ar-Ar ages as low as 4506 ± 15 Myr implies that some clasts were acquired over a period of ≥50 Myr (Turrin et al. 2015), not solely during the reaccretion of the ureilite parent body.

Iron meteorites, from both carbonaceous and non-carbonaceous isotopic reservoirs, also bear witness to catastrophic impact events that separated core and mantle material early in the solar system history (Scott et al. 2015). None can be definitely associated with the intense spike in the frequency and velocity of impacts associated with the Grand Tack. However, we are optimistic that the rich impact record of meteorites will allow more definitive tests of the Grand Tack model and the role of the giant planets in forming and mixing the two isotopic populations.

6. Summary and Conclusions

Nucleosynthetic isotopic variations are ubiquitous in whole meteorites and probably reflect thermal processing of presolar grains and phases that inherited the isotopic signatures of presolar grains. The nucleosynthetic variations and mass-independent oxygen isotopic effects reveal an isotopic dichotomy among meteorites that is shown by chondrites as well as all kinds of differentiated meteorites, including achondrites, pallasites, and iron meteorites. Inferred accretion times show that the dichotomy existed in the disk for most of its lifetime: from accretion of the oldest iron meteorites at ~0.2 Myr after CAIs to the accretion of the

youngest carbonaceous chondrites around 3–4 Myr after CAIs (Kruijer et al. 2017). The two isotopic populations must therefore have coexisted in the disk separated most plausibly by proto-Jupiter.

Carbonaceous chondrites differ from the other chondrites—ordinary, enstatite, R (Rumuruti), and K (Kakangari) chondrites—as they accreted more water and refractory inclusions. The latter were probably ejected from close to the Sun, possibly by disk winds, carried beyond the region where the giant planets formed, and spiraled in under gas drag. Once proto-Jupiter reached a mass of 10–20 $M_{\oplus}$, it would have begun to accrete gas so that the gas pressure was locally depleted. In the zone with a reversed pressure gradient, millimeter- and centimeter-sized refractory inclusions and ice particles would have migrated outward. This process would have kept the inner solar system deficient in refractory materials, which are ^{16}O-rich, and ice, which is ^{16}O-poor, and it would account for the enhanced bulk refractory abundances of carbonaceous chondrites, as well as their positive ε^{50}Ti values (CAIs have high ε^{50}Ti values). Chondrules in carbonaceous chondrites have large spreads in their Δ^{17}O and ε^{50}Ti values because they were contaminated with refractory grains and because of the presence of isotopically heavy ice. Chondrules in ordinary, enstatite, R, and K chondrites have oxygen isotopic compositions that lie close to the terrestrial fractionation line on the three-isotope plot. Their ε^{50}Ti values show little scatter because CAIs were deficient in the inner solar system (Gerber et al. 2017). Differences between the isotopic compositions of chondrules in carbonaceous and non-carbonaceous chondrites strongly support the suggestion that Jupiter was responsible for the isotopic dichotomy among meteorites (Warren 2011a, 2011b).

The two isotopic populations may have been mixed together when Jupiter and Saturn migrated inward emptying the asteroid belt and then repopulating it with roughly equal masses of asteroids from the two populations (Walsh et al. 2011). The approximately 0.5 Myr spike in the impact flux and velocity during the Grand Tack may have caused the hypervelocity impact that created the CB chondrites from an impact-generated gas-melt plume (Johnson et al. 2016). The presence of clasts of ordinary chondrite in the CB chondrites, Bencubbin and Weatherford (Weisberg et al. 1990) shows that ordinary chondrite fragments were present in the belt along with CAIs when the plume materials accreted. The Grand Tack may also have caused the disruption of the ureilite parent body. Nebular gas and pebble accretion would have enabled the meter-sized ureilite fragments to reaccrete over a longer period after they had cooled. The extraordinary variety of clasts in the Almahata Sitta ureilite breccia can plausibly be attributed to this unique period in solar system history.

The classical concept of a highly stratified asteroid belt in which diverse kinds of meteorites formed in situ in specific zones is inconsistent with the isotopic dichotomy. The asteroid belt is a “cosmic zoo” that contains planetesimals from all over the solar system: enstatite chondrites and achondrites and winonaites, which isotopically resemble the Earth, from <2 au and carbonaceous chondrites from beyond Jupiter. The S-type asteroids formed in the asteroid belt, but the P- and D-type asteroids, which dominate at 4–5 au appear to have been added later from beyond Neptune, probably during the giant planet instability (Vokrouhlickyí et al. 2016).

The abundance of CAIs and chondrules as fragments in returned samples of comet 81P/Wild 2 does not require large-scale transport of chondritic ingredients across the disk. Chondrules probably formed throughout the giant planet region. Refractory inclusions appear to be ubiquitous in all bodies that formed in the outer solar system, consistent with dispersion by disk winds.

Acknowledgments

This work was partly supported by the National Aeronautics and Space Administration (NASA) Cosmochemistry grant NNX10AH76G (ANK, PI) and NASA Emerging Worlds grant NNX15AH38G (ANK, PI). We thank Fred Ciesla, Jonathan Williams, and many other colleagues for helpful discussions, and Joe Nuth for very thorough reviews.

Appendix

Meteorite Data

Table 1 shows the names of the meteorite groups that are plotted in Figures 2 and 3 and the sources of data for Figure 2.

References

Akram W, Schönbachler M, Bisterzo S, & Gallino R 2015, GeCoA, 165, 484

Alexander CMO'D 2017, RSPTA, 375, 20150384

Alexander CMO'D, Bowden R, Fogel ML, et al. 2012, Sci, 337, 721

Alexander CMO'D, Nittler LR, Davidson J, & Ciesla FJ 2016, M&PSA, 51, 6351

Barrat JA, Dauphas N, Gillet P, et al. 2016, GeCoA, 176, 1

Barrat JA, Greenwood RC, Verchovsky AB, et al. 2015, GeCoA, 168, 280

Bell JF, Davis DR, Hartmann WK, & Gaffey MJ 1989, in Asteroids II, ed. Binzel RP et al. (Tucson: Univ. Arizona Press),921

Bischoff A, Horstmann M, Barrat J-A, et al. 2014, PNAS, 111, 12689 [PubMed: 25136108]

Bischoff A, Vogel N, & Roszjar J 2011, ChEG, 71, 101

Bjerkeli P, van der Wiel MHD, Harsono D, Ramsey JP, & Jørgenson JS 2016, Natur, 540, 406

Bogdanovski O, & Lugmair GW 2004, LPI, 35, 1715

Bollard J, Connelly JN, & Bizzarro M 2015, M&PS, 50, 1197

Bottke WF, Nesvorny D, Grimm RE, Morbidelli A, & O'Brien DP 2006, Natur, 439, 821

Bottke WF, Vokrouhlicky D, Rubincam DP, & Broz M 2002, in Asteroids III, ed. Bottke WF et al. (Tucson: Univ. Arizona Press),395

Brasser R, & Morbidelli A 2013, Icar, 225, 40

Brennecka GA, Borg LE, & Wadhwa M 2013, PNAS, 110, 17241 [PubMed: 24101483]

Brownlee D 2014, AREPS, 42, 179

Brownlee D, Joswiak D, & Matrajt G 2012, M&PS, 47, 453

Budde G, Burkhardt C, Brennecka GA, et al. 2016a, E&PSL, 454, 293

Budde G, Kleine T, Kruijer TS, Burkhardt C, & Metzler K 2016b, PNAS, 113, 2886 [PubMed: 26929340]

Budde G, Kruijer TS, & Kleine T 2017, LPI, 48, 1886

Burbine TH 2014, in Treatise on Geochemistry, ed. Davis AM (2nd ed.; Oxford: Elsevier),365

Burkhardt C, Dauphas N, Tang H, et al. 2015, LPI, 46, 2732

Burkhardt C, Kleine T, Dauphas N, & Wieler R 2012, E&PSL, 357–8, 298

Burkhardt C, Kleine T, Oberli F, et al. 2011, E&PSL, 312, 390

Burkhardt C, & Schönbachler M 2015, GeCoA, 165, 361
Chaumard N, Defouilloy C, & Kita NT 2016, M&PSA, 51, 6408
Chaumard N, Defouilloy C, Kita NT, & Hertwig A 2017, LPI, 48, 1610
Choi B-G, McKeegan KD, Krot AN, & Wasson JT 1998, Natur, 392, 577
Ciesla F 2007, Sci, 318, 613
Ciesla F 2010, Icar, 208, 455
Clayton RN 2002, Natur, 415, 860
Clayton RN 2004, in Treatise on Geochemistry, Vol. 1, ed. Davis AM (Oxford: Elsevier),129
Clayton RN, Grossman L, & Mayeda TK 1973, Sci, 182, 485
Clayton RN, & Mayeda TK 1996, GeCoA, 60, 1999
Connelly JN, Bizzarro M, Krot AN, et al. 2012, Sci, 338, 651
Cuzzi JN, Davis SS, & Dobrovolskis AR 2003, Icar, 127, 290
Dauphas N, Marty R, & Reisberg L 2002, ApJ, 565, 640
Dauphas N, & Pourmand A 2015, GeCoA, 163, 234
Dauphas N, Remusat L, Chen JH, et al. 2010, ApJ, 720, 1577
Dauphas N, & Schauble EA 2016, AREPS, 44, 709
Davidsson BJR, Sierks H, Güttler C, et al. 2016, A&A, 592, A63
Davis AM, Zhang J, Hu J, Greber ND, & Dauphas N 2016, LPI, 47, 3023
Day JMD, Walker RJ, Ash RD, et al. 2012, GeCoA, 81, 94
De Meo FE, & Carry B 2014, Natur, 505, 629
Desch SJ, Morris MA, Connolly HC, & Boss AP 2010, ApJ, 725, 692
Dominguez G 2010, ApJL, 713, L59
Doyle PM, Jogo K, Nagashima K, et al. 2015, NatCo, 6, 7444, http://www.nature.com/articles/ncomms8444
Ebel DS, Brunner C, Konrad K, et al. 2016, GeCoA, 172, 322
Fioretti AM, Goodrich CA, Shaddad M, et al. 2017, LPI, 48, 1846
Fischer-Gödde M, Burkhardt C, Kruijer TS, & Kleine T 2015, GeCoA, 168, 151
Floss C, Taylor LA, Promprated P, & Rumble D 2005, M&PS, 40, 343
Franchi IA, Baker L, Bridges JC, Wright IP, & Pillinger CT 2001, RSPTA, 359, 2019
Frank DR, Huss GR, Nagashima K, Zolensky ME, & Le L 2017, M&PSA, 52, 6355
Frank DR, Zolensky ME, & Le L 2014, GeCoA, 142, 240
Gardner-Vandy KG, Lauretta DS, Greenwood RC, et al. 2012, GeCoA, 85, 142
Gerber S, Burkhardt C, Budde G, Metzler K, & Kleine T 2017, ApJL, 841, L17
Ghosh A, Weidenschilling SJ, McSween HY, & Rubin A 2006, in Meteorites and the Early Solar System, ed. Lauretta DS & McSween HY (Tucson: Univ. Arizona Press),555
Goodrich C, Hartmann WK, O'Brien DP, et al. 2015, M&PS, 50, 782
Goodrich CA, Kita NT, Yin QZ, et al. 2017, GeCoA, 203, 381
Goodrich CA, Scott ERD, & Fioretti AM 2004, ChEG, 64, 283
Göpel C, Birck J-L, Galy A, Barrat J-A, & Zanda B 2015, GeCoA, 156, 1
Gounelle M, Morbidelli A, Bland PA, et al. 2008, in The Solar System Beyond Neptune, ed. Barucci MA et al. (Tucson: Univ. Arizona Press),525
Gradie JC, & Tedesco EF 1982, Sci, 216, 1405
Greenwood RC, Barrat J-A, Scott ERD, et al. 2015, GeCoA, 169, 115
Greenwood RC, Burbine TH, Miller MF, & Franchi IA 2017, ChEG, 77, 1
Greenwood RC, Franchi IA, Gibson JM, & Benedix GK 2012, GeCoA, 94, 146
Greenwood RC, Franchi IA, Jambon A, & Buchanan PC 2005, Natur, 435, 916
Grimm RE, & McSween HY 1993, Sci, 259, 653
Haack H, Scott ERD, Love SG, Brearley AJ, & McCoy TJ 1996, GeCoA, 60, 3103

Helled R, Bodenheimer P, Podolak M, et al. 2013, in Protostars & Planets VI, ed. Beuther Het al. (Tucson: Univ. Arizona Press),643

Herrin JS, Zolensky ME, Ito M, et al. 2010, M&PS, 45, 1789

Hertwig A, Defouilloy C, & Kita NT 2016, M&PSA, 51, 6472

Hezel DC, Russell SS, Ross AJ, & Kearsley AT 2008, M&PS, 43, 1879

Hibiya Y, Archer GJ, Tanaka R, et al. 2017, LPI, 48, 1319

Horstmann M, & Bischoff A 2014, ChEG, 74, 149

Jacquet E 2014, CRGeo, 346, 3

Jacquet E, Barrat JA, Beck P, et al. 2016, M&PS, 51, 851

Jacquet E, Gounelle M, & Fromang S 2012, Icar, 220, 162

Johansen A, Mac Low MM, Lacerda P, & Bizzarro M 2015, SciA, 1, e1500109

Johnson BC, Walsh KJ, Minton DA, Krot AN, & Levison HF 2016, SciA, 2, e1601658

Jones RH 2012, M&PS, 47, 1176

Joswiak DJ, Brownlee DE, Nguyen AN, & Messenger S 2017, M&PS, 52, 1612

Kallemeyn GW, Rubin AE, & Wasson JT 1994, GeCoA, 58, 2873

Kita NT, Kimura M, Ushikubo T, Valley JW, & Nyquist L 2008, LPI, 39, 2059

Kita NT, Nagahara H, Tachibana S, et al. 2010, GeCoA, 74, 6610

Kita NT, Tenner TJ, Defoouilloy C, et al. 2015, LPI, 46, 1455

Kita NT, Tenner TJ, Nakashima D, Ushikubo T, & Bischoff A 2013, M&PSA, 48, 5149

Kita NT, & Ushikubo T 2012, M&PS, 47, 1108

Kleine K, & Wadhwa M 2017, in Planetesimals: Early Differentiation and Consequences for Planets, ed. Elkins-Tanton LT & Weiss BP (Cambridge: Univ. Cambridge Press),224

Kööp L, Davis AM, Nakashima D, Park C, et al. 2016, GeCoA, 189, 70

Kretke KA, Bottke W, Kring DA, & Levison HF 2017, AAS DDA meeting, 48, 103.02

Krot AN, Amelin Y, Bland P, et al. 2009, GeCoA, 73, 4963

Krot AN, Keil K, Scott ERD, Goodrich CA, & Weisberg MK 2014, in Treatise on Geochemistry, ed. Davis AM (2nd ed.; Oxford: Elsevier),1

Krot AN, Libourel G, & Chaussidon M 2006, GeCoA, 70, 767

Krot AN, Nagashima K, Alexander CMO'D, et al. 2015, in Asteroids IV, ed. Michel P, De Meo FE, & Bottke WF (Tucson: Univ. Arizona Press),635

Krot AN, & Nagashima K 2017, GeocJ, 51, 45

Krot AN, Nagashima K, Ciesla FJ, et al. 2010, ApJ, 713, 1159

Kruijer TS, Burkhardt C, Budde G, & Kleine T 2017, PNAS, 114, 6712 [PubMed: 28607079]

Lambrechts M, Johansen A, & Morbidelli A 2014, A&A, 572, A35

Leshin LA, Rubin AE, & McKeegan KD 1997, GeCoA, 61, 835

Leya I, Schönbächler M, Krähenbühl U, & Halliday AN 2009, ApJ, 702, 1118

Liffman K, Cuello N, & Patterson DA 2016, MNRAS, 462, 1137

Lin Y, Kimura M, Miao B, Dai D, & Monoi A 2006, M&PS, 41, 67

Lissauer JJ, Hubickyj O, D'Angelo G, & Bodenheimer P 2009, Icar, 199, 338

Lugaro M, Liffman K, Ireland TR, & Maddison ST 2012, ApJ, 759, 51

Lyons JR, & Young ED 2005, Natur, 435, 317

MacPherson GJ 2014, in Treatise on Geochemistry, ed. Davis AM (2nd ed.; Oxford: Elsevier),139

Makide K, Nagashima K, Krot AN, et al. 2009, GeCoA, 73, 5018

Makide K, Nagashima K, Krot AN, et al. 2011, ApJL, 733, L31

Mayer B, Wittig N, Humayun M, & Leya I 2015, ApJ, 809, 180

McCulloch MT, & Wasserburg GJ 1978, ApJL, 220, L15

McDermott KH, Greenwood RC, Scott ERD, Franchi IA, & Anand M 2016, GeCoA, 173, 97

McKeegan KD, Chaussidon M, & Robert F 2000, Sci, 289, 1334

McKeegan KD, Kallio APA, Heber VS, et al. 2011, Sci, 332, 1528

McSween HY, & Huss GR 2010, Cosmochemistry (Cambridge: Univ. Cambridge Press),548

Morbidelli A, Bitsch B, Crida A, et al. 2016, Icar, 267, 318

Morbidelli A, & Raymond SN 2016, JGRE, 121, 1962

Morbidelli A, Walsh KJ, O'Brien DP, Minton DA, & Bottke WF 2015, in Asteroids IV, ed. Michel P, De Meo FE, & Bottke WF (Tucson: Univ. Arizona Press),493

Morlok A, Bischoff A, Stephan T, et al. 2006, GeCoA, 70, 5371

Nagashima K, Kita NT, & Luu T-H 2018, Chondrules and the Protoplanetary Disk (Oxford: Elsevier)

Nagashima K, Krot AN, & Huss GR 2015, GeCoA, 151, 49

Nakamura T, Noguchi T, Tanaka M, et al. 2011, Sci, 333, 1113

Nakashima D, Ushikubo T, Joswiak DJ, et al. 2012, E&PSL, 357, 355

Niederer FR, & Papanastassiou D 1984, GeCoA, 48, 1279

Niemeyer S 1985, GRL, 12, 733

Niemeyer S 1988, GeCoA, 52, 2941

Niemeyer S, & Lugmair GW 1984, GeCoA, 48, 1401

Nuth JA, Paquette JA, & Farquhar A 2012, M&PS, 47, 2056

O'Brien DP, Morbidelli A, & Bottke WF 2007, Icar, 191, 434

Ogliore RC, Huss GR, Nagashima K, et al. 2012, ApJL, 745, L19

Olsen MB, Wielandt D, Schiller M, Van Kooten EMME, & Bizzarro M 2016, GeCoA, 191, 118

Oulton J, Humayun M, Fedkin A, & Grossman L 2016, GeCoA, 177, 254

Palme H, Lodders K, & Jones A 2014, in Treatise on Geochemistry, ed. Davis AM (2nd ed.; Oxford: Elsevier),15

Park C, Nagashima K, Krot AN, et al. 2017, GeCoA, 201, 6

Peters STM, Munker C, Pfeifer M, & Elfers B-M 2017, E&PSL, 459, 70

Poole GM, Rehkämper M, Coles BJ, Goldberg T, & Smith CL 2017, E&PSL, 473, 215

Pringle EA, Moynier F, Beck P, Paniello R, & Hezel DC 2017, E&PSL, 468, 62

Prinz M, Weisberg MK, Clayton RN, & Mayeda TK 1993, Metic, 28, 419

Prombo C, & Lugmair GW 1987, Metic, 22, 483

Qin L, Alexander CM, Carlson RW, Horan MF, & Yokoyama T 2010, GeCoA, 74, 1122

Raymond SN, & Izidoro A 2017, Icar, 297, 134

Rubin AE 2011, Icar, 213, 547

Ruiz-Rodriguez D, Cierza LA, Williams JP, et al. 2017, MNRAS, 468, 3266

Sahijpal S, & Goswami JN 1998, ApJL, 509, L137

Sakamoto N, Seto Y, Itoh S, et al. 2007, Sci, 317, 231

Salmeron R, & Ireland TR 2012, E&PSL, 327–8, 61

Sanborn ME, & Yin Q-Z 2015, LPI, 46, 2241

Sanborn ME, Yin Q-Z, & Irving AJ 2014, LPI, 45, 2032

Sanborn ME, Yin Q-Z, Irving AJ, & Bunch TE 2015, LPI, 46, 2259

Sanborn ME, Yin Q-Z, & Mittlefehldt DW 2016a, LPI, 47, 2256

Sanborn ME, Yin Q-Z, Schmitz B, & Amelin Y 2016b, LPI, 47, 2309

Schmitz B, Yin Q-Z, & Sanborn ME 2016, NatCo, 7, 11851

Schoenbeck TW, Kleine T, & Irving AJ 2005, LPI, 37, 1550

Schrader DL, Nagashima K, Krot AN, Ogliore RC, & Hellebrand C 2014, GeCoA, 132, 50

Scott ERD, Greenwood RC, Franchi IA, & Sanders IS 2009, GeCoA, 73, 5835

Scott ERD, Keil K, Goldstein JI, et al. 2015, in Asteroids IV, ed. Michel P, De Meo FE, & Bottke WF (Tucson: Univ. Arizona Press),573

Scott ERD, & Krot AN 2005, in ASP Conf. Ser. 341, Chondrules & the Protoplanetary Disk, ed. Krot AN, Scott ERD, & Reipurth B (San Francisco, CA: ASP),15

Scott ERD, & Krot AN 2014, in Treatise on Geochemistry, ed. Davis AM (2nd ed.; Oxford: Elsevier), 65

Seto Y, Sakamoto N, Fujino K, et al. 2008, GeCoA, 72, 2723
Shu FH, Shang H, & Lee T 1996, Sci, 271, 155
Shukolyukov A, & Lugmair GW 2006, E&PSL, 250, 200
Steele RCJ, Coath CD, Regelous M, Russell S, & Elliott T 2012, ApJ, 758, 59
Steele RCJ, Elliott T, Coath CD, & Regelous M 2011, GeCoA, 75, 7906
Stracke A, Palme H, Gellissen M, et al. 2012, GeCoA, 85, 114
Sugiura N, & Fujiya W 2014, M&PS, 49, 772
Tenner TJ, Kimura M, & Kita NT 2017, M&PS, 52, 268
Tenner TJ, Nakashima D, Ushikubo T, Kita NT, & Weisberg MK 2015, GeCoA, 148, 228
Trinquier A, Birck J-L, & Allegre CJ 2007, ApJ, 655, 1179
Trinquier A, Elliott T, Ulfbeck B, et al. 2009, Sci, 324, 374
Turrin BD, Lindsay FN, Herzog GF, et al. 2015, LPI, 46, 2784
Ushikubo T, Kimura M, Kita NT, & Valley JW 2012, GeCoA, 90, 242
Van Kooten EMME, Wielandt D, Schiller M, et al. 2016, PNAS, 113, 2011 [PubMed: 26858438]
Vokrouhlickyí D, Bottke WF, & Nesvornyí D 2016, ApJ, 152, 39
Walsh KJ, Morbidelli A, Raymond SN, O'Brien DP, & Mandell A 2011, Natur, 475, 206
Walsh KJ, Morbidelli A, Raymond SN, O'Brien DP, & Mandell A 2012, M&PS, 47, 1941
Warren PH 2011a, GeCoA, 75, 6912
Warren PH 2011b, E&PSL, 311, 93
Warren PH, Rubin AE, Isa J, et al. 2013, GeCoA, 107, 135
Weidenschilling SJ 1977, MNRAS, 180, 57
Weisberg MK, Ebel DS, Connolly HC, Kita NT, & Ushikubo T 2011, GeCoA, 75, 6556
Weisberg MK, Prinz M, Clayton RN, et al. 1996, GeCoA, 60, 4253
Weisberg MK, Prinz M, & Nehru CE 1990, Metic, 25, 289
Westphal AJ, Fakra SC, Gainsforth Z, et al. 2009, ApJ, 694, 18
Worsham E, Bermingham KR, & Walker RJ 2017, E&PSL, 467, 157
Yamaguchi A, Clayton RN, Mayeda TK, et al. 2002, Sci, 296, 334
Yamakawa A, Yamashita K, Makashima A, & Nakamura E 2010, ApJ, 720, 150
Yin Q-Z, Yamashita K, Yamakawa A, et al. 2009, LPI, 40, 2006
Yurimoto H, & Kuramoto K 2004, Sci, 305, 1763
Zhao X, Floss C, Lin Y, & Bose M 2013, ApJ, 769, 49
Zinner E 2014, in Treatise on Geochemistry, ed. Davis AM (2nd ed.; Oxford: Elsevier),181

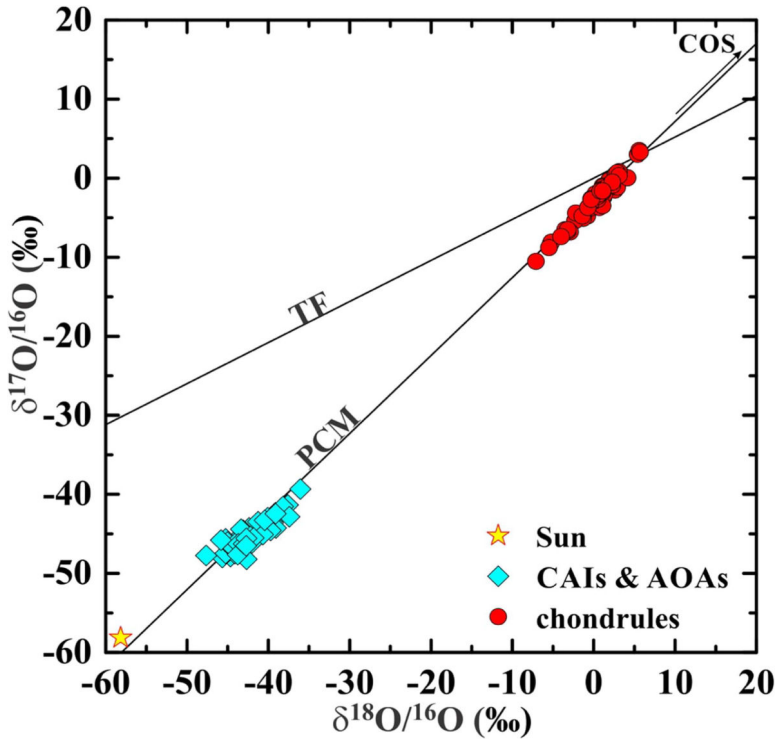

Figure 1.

Plot of $\delta^{17}O/^{16}O$ vs. $\delta^{18}O/^{16}O$ showing oxygen isotopic compositions of chondrules and two kinds of refractory inclusions—calcium-aluminum-rich inclusions (CAIs) and amoeboid olivine aggregates (AOAs)—in the CR group of carbonaceous chondrites, which are the least metamorphosed and altered chondrites. The isotopic ratios are plotted as permil deviations from the standard. Since chondrules and refractory inclusions have such different compositions, they probably formed in two very distinct regions in the disk: an ^{16}O-rich solar-like region for refractory inclusions and an ^{16}O-poor planetary-like location for chondrules. The primitive chondrule mineral line (PCM; Ushikubo et al. 2012) intersects with the terrestrial fractionation line (TF) close to the composition of the terrestrial mantle, lunar rocks, and E chondrites, and can be extended to the extremely ^{16}O-poor cosmic symplectites (COS; Seto et al. 2008), bulk CAIs and AOAs, and the inferred composition of the Sun (McKeegan et al. 2011). Data from Krot et al. (2006), Makide et al. (2009) Schrader et al. (2014), and Tenner et al. (2015).

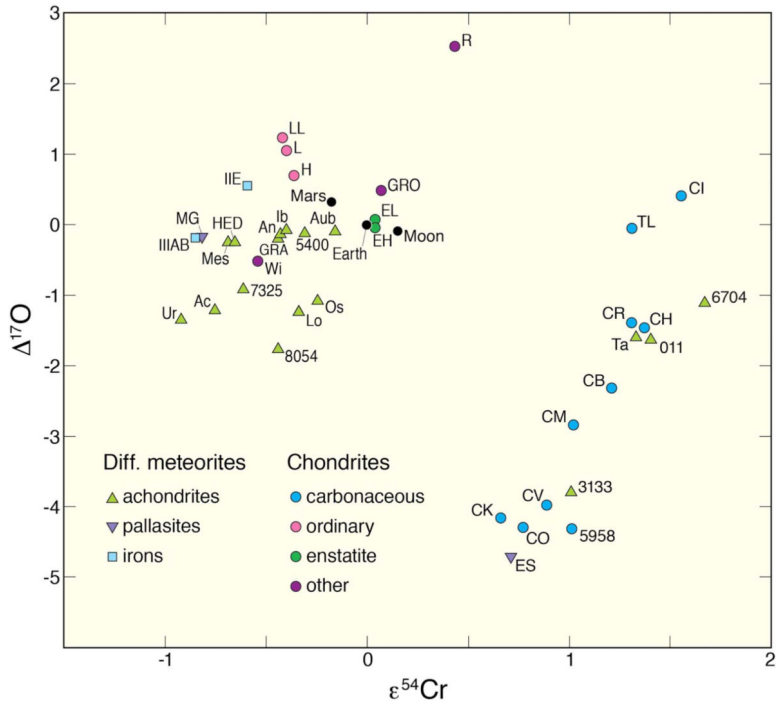

Figure 2.

Plot of the mass-independent isotopic parameters $\Delta^{17}O$ vs. $\varepsilon^{54}Cr$ for chondrites, differentiated meteorites, and planets showing that they are derived from two very distinct isotopic reservoirs. Carbonaceous chondrites and a few differentiated meteorites plot on the right; other chondrites and most differentiated meteorites, the Earth, Mars, and the Moon plot on the left side. $\varepsilon^{54}Cr$ is the deviation of $^{54}Cr/^{52}Cr$ in parts per 10^4 from terrestrial Cr, assuming that the $^{52}Cr/^{50}Cr$ ratios are terrestrial. $\Delta^{17}O$ is the vertical deviation from the terrestrial fractionation line on the three-isotope plot (Figure 1): $\Delta^{17}O = \delta^{17}O–0.52\delta^{18}O$. For abbreviations and data sources, see the Appendix.

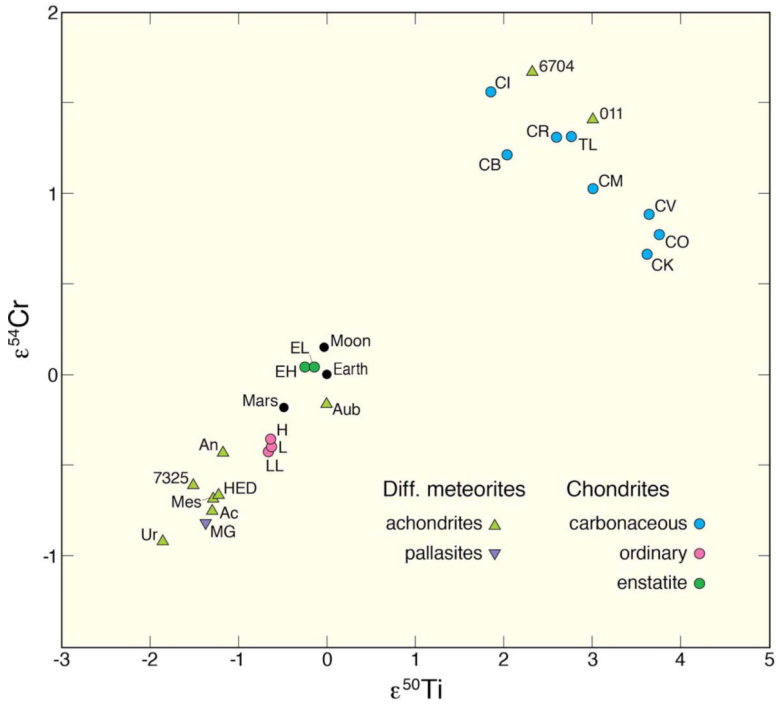

Figure 3.

Plot of ε^{54}Cr vs. ε^{50}Ti, which is the deviation of ^{50}Ti/^{47}Ti in parts per 10^4 from terrestrial Ti, for chondrites, differentiated meteorites, and planets, assuming that the ^{49}Ti/^{47}Ti ratios are terrestrial. Carbonaceous chondrites and two achondrites, which formed in the outer solar system, are isotopically quite distinct from other chondrites, most differentiated meteorites, and Earth, Mars, and the Moon, which formed in the inner solar system. For abbreviations of meteorite names and groups, see the Appendix. Data from Dauphas & Schauble (2016) and sources in the Appendix.

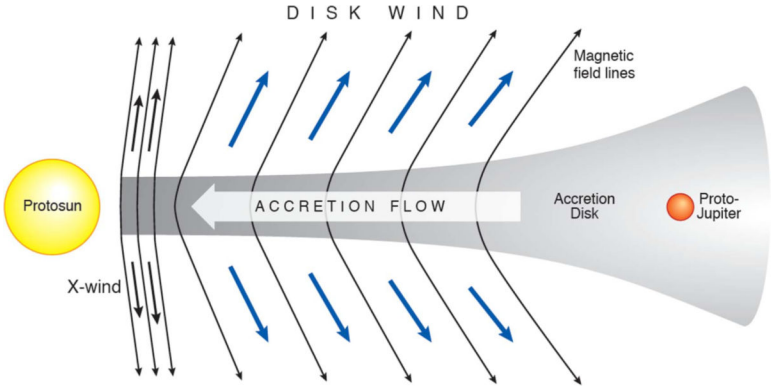

Figure 4.

Cartoon showing the protosolar disk, which surrounds the young Sun, and two mechanisms that have been proposed to accelerate ionized gas along magnetic field lines and launch refractory inclusions and chondrules to the outer part of the disk: the X-wind from close to the protostar (Shu et al. 1996) and disk winds (Salmeron & Ireland 2012). The X-wind model has many problems (Krot et al. 2009; Desch et al. 2010). However, ALMA observations suggest that disk winds, which are responsible for removing angular momentum from disks, may have ejected refractory inclusions to the disk periphery (Bjerkeli et al. 2016). Early growth of proto-Jupiter to ~15 M_e could have prevented refractory inclusions from spiraling back into the inner solar system so that they survived in the disk for several megayears (after Salmeron & Ireland 2012).

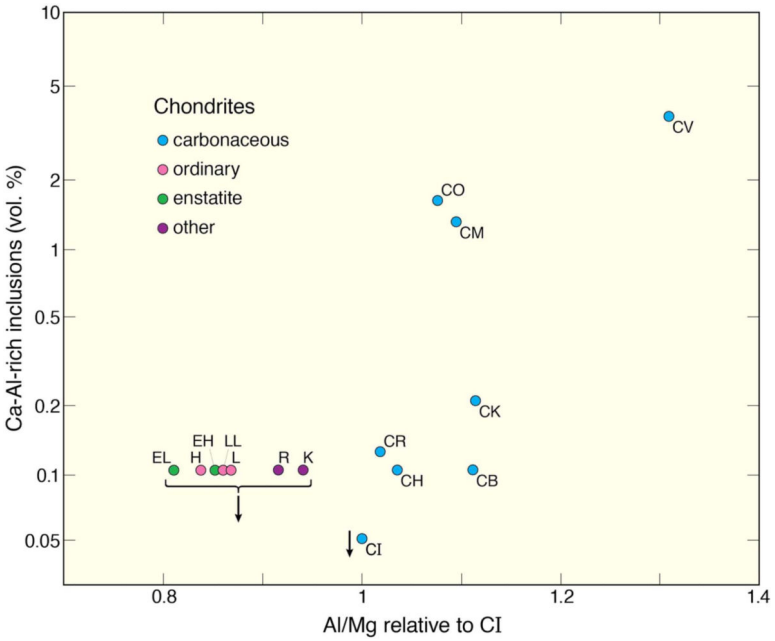

Figure 5.

Plot showing the volume of Ca–Al-rich inclusions in chondrite groups plotted against the Al/Mg ratio normalized to the CI chondrite ratio. The enhanced abundance of Al (and other refractory elements) in carbonaceous chondrites probably results from the addition of CAIs, which are scarce in ordinary, enstatite, and other chondrites. CI chondrites are heavily brecciated and altered and probably once contained more CAIs (see the text). Data are from Scott & Krot (2005), Hezel et al. (2008), and Ebel et al. (2016), and the Al/Mg ratio of CR chondrites is from Kallemeyn et al. (1994).

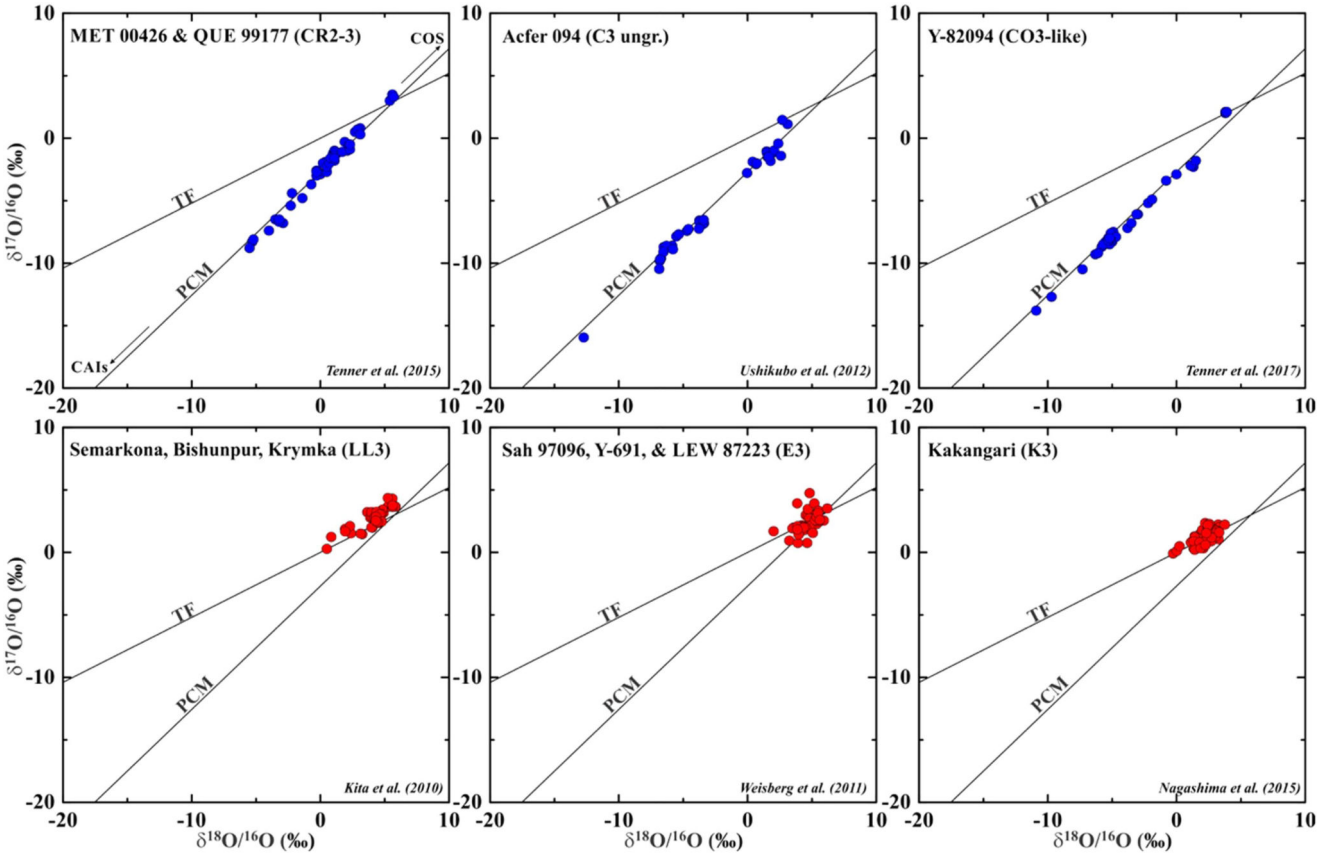

Figure 6.

Plots of $\delta^{17}O/^{16}O$ vs. $\delta^{18}O/^{16}O$ showing oxygen isotopic compositions of olivine and pyroxene in chondrules in three types of carbonaceous chondrites— CR2–3 chondrites (Tenner et al. 2015), ungrouped C3 carbonaceous chondrite, Acfer 094 (Ushikubo et al. 2012), and the CO3-like chondrite Y 82094 (Tenner et al. 2017), and three types of non-carbonaceous chondrites—LL ordinary chondrites (Kita et al. 2010), EH3 and EL3 enstatite chondrites (Weisberg et al. 2011), and the K3 chondrite, Kakangari (Nagashima et al. 2015). Chondrules in carbonaceous chondrites have oxygen isotopic compositions that spread along the slope 1 primitive chondrule mineral line (PCM), probably due to the abundance of ^{16}O-rich refractory materials and relatively ^{16}O-poor water in the outer solar system. Chondrules in non-carbonaceous chondrites plot close to the slope 1/2 terrestrial mass fractionation line (TF), consistent with the deficiency of water and refractory material in the inner solar system and an initial Earth-like oxygen isotopic composition for anhydrous solar system silicates. Data from chondrules that contain isotopically distinct grains have been omitted.

Table 1

Meteorite Groups and Sources of Data for Figures 2 and 3

Symbol	Name	$\Delta^{17}O$ Reference	$E^{54}Cr$ Reference
Inner Solar System			
Chondrites			
EH, EL	Enstatite	Dauphas & Schauble (2016)	Dauphas & Schauble (2016)
H, L, LL	Ordinary	Dauphas & Schauble (2016)	Dauphas & Schauble (2016)
R	Rumuruti-type	Dauphas & Schauble (2016)	Qin et al. (2010)
Wi	Winonaite	Greenwood et al. (2012)	Schmitz et al. (2016)
GRO	GRO 95551	Warren (2011b)	Qin et al. (2010)
Achondrites			
Ac	Acapulcoite	Dauphas & Schauble (2016)	Dauphas & Schauble (2016)
An	Angrite	Greenwood et al. (2017)	
Au	Aubrite (enstatite ach.)	Dauphas & Schauble (2016)	Dauphas & Schauble (2016)
Lo	Lodranite	Dauphas & Schauble (2016)	Dauphas & Schauble (2016)
HED	Howardite, eucrite, diogenite	Greenwood et al. (2005)	Dauphas & Schauble (2016)
Mes	Mesosiderite	Greenwood et al. (2015)	Dauphas & Schauble (2016)
Ur	Ureilite	Dauphas & Schauble (2016)	Yamakawa et al. (2010)
Ib	Ibitira	Scott et al. (2009)	Sanborn et al. (2016a)
GRA	GRA 06128	Day et al. (2012)	Sanborn & Yin (2015)
Os	Osterplana 065	Schmitz et al. (2016)	Schmitz et al. (2016)
5400	NWA 5400	Burkhardt et al. (2015)	Sanborn et al. (2016b)
7325	NWA 7325	Barrat et al. (2015)	Goodrich et al. (2017)
8054	NWA 8054	Sanborn et al. (2014)	Sanborn et al. (2014)
Others			
IIE	IIE iron	McDermott et al. (2016)	Trinquier et al. (2007)
IIIAB	IIIAB iron	Dauphas & Schauble (2016)	Trinquier et al. (2007)
MG	Main group pallasite	Greenwood et al. (2015)	Trinquier et al. (2007) Qin et al. (2010)
Mars		Franchi et al. (2001)	Dauphas & Schauble (2016)
Moon		Dauphas & Schauble (2016)	Dauphas & Schauble (2016)
Outer Solar System			

Symbol	Name	$\Delta^{17}O$ Reference	$E^{54}Cr$ Reference
Chondrites			
CB, CI, CK, CM, CO, CV, CR	Carbonaceous	Dauphas & Schauble (2016)	Dauphas & Schauble (2016)
TL	Tagish Lake	Yin et al. (2009)	Yin et al. (2009)
Achondrites			
Ta	Tafassasset	Gardner-Vandy et al. (2012)	Göpel et al. (2015)
011	NWA 011	Floss et al. (2005) Yamaguchi et al. (2002)	Bogdanovski & Lugmair (2004)
3133	NWA 3133	Schoenbeck et al. (2005)	Sanborn et al. (2015)
5958	NWA 5958	Jacquet et al. (2016)	Göpel et al. (2015)
6704	NWA 6704 (also 6693)	Warren et al. (2013)	Hibiya et al. (2017)
Other			
ES	Eagle Station pallasite	Clayton & Mayeda (1996)	Shukolyukov & Lugmair (2006)